energies

MDPI

Article

Experimental Investigation on Performance of an Organic Rankine Cycle System Integrated with a Radial Flow Turbine

Lisheng Pan [1,2] and Huaixin Wang [2,*]

1 State Key Laboratory of High-temperature Gas Dynamics, Institute of Mechanics, Chinese Academy of Sciences, Beijing 100190, China; panlisheng@imech.ac.cn
2 Department of Thermal Energy and Refrigeration Engineering, Tianjin University, Tianjin 300072, China
* Correspondence: wanghx@tju.edu.cn; Tel.: +86-22-2740-5049

Received: 5 January 2019; Accepted: 19 February 2019; Published: 22 February 2019

Abstract: An experimental method is used to investigate the performance of a small-scale organic Rankine cycle (ORC) system which is integrated with a radial flow turbine, using 90 °C hot water as a heat source. The considered working fluids are R245fa and R123. The relationship between cycle performance and the operation parameters is obtained. With constant condensing pressure (temperature), the outlet temperature of the hot water, the mass flow rate of the hot water and the evaporator heat transfer rate increase with increasing evaporating pressure. Turbine isentropic efficiency decreases and transmission-generation efficiency increases with rising evaporating pressure. In the considered conditions, the maximum specific energy is 1.28 kJ/kg, with optimal fluid of R245fa and an optimal evaporating temperature of 69.2 °C. When the evaporating pressure (temperature) is constant, the outlet temperature of the cooling water increases, and the mass flow rate of the cooling water decreases with increasing condensing pressure. Turbine isentropic efficiency increases and transmission-generation efficiency decreases with the rise of condensing pressure. In the considered conditions, the maximum specific energy is 0.89 kJ/kg, with optimal fluid of R245fa and an optimal condensing temperature of 29.1 °C. Turbine efficiency is impacted by the working fluid type, operation parameters and nozzle type.

Keywords: organic Rankine cycle (ORC); system performance; radial flow turbine; experimental study

1. Introduction

A great amount of researcher attention has been focused on exploiting or recovering low-grade heat energy using the organic Rankine cycle (ORC), which has potential in using low-grade heat energy (approximately 100–150 °C). This grade of heat energy is very common in nature and society, including low temperature geothermal energy and industrial waste heat. In addition, solar thermal energy, produced by moderately low temperature solar collectors, is also important renewable low-grade energy. The working fluid type, operation parameters and expander performance play major roles in determining the ORC system performance.

Much research was carried out on the optimization of the working fluid and the operation parameters. Tchanche et al. [1] studied the theoretical cycle performance of a 2 kW micro ORC system using 90 °C hot water as a heat source, produced by solar collectors. Several characteristics, such as efficiencies, volume flow rate, mass flow rate, pressure ratio, toxicity, flammability, ozone depression potential (ODP) and global warming potential (100 year) (GWP) were considered to screen an optimal fluid from as many as 20 fluids. The results showed that R134a was most suitable for small-scale solar

applications. When dry fluid (with a positive slope for the saturated gas line) is used, especially in high evaporating temperature conditions, cycle exergy efficiency can be improved by a regenerator, where the effect is fluid dependent [2]. Madhawa Hettiarachchi et al. [3] proposed an economic objective function to screen optimal fluids for low temperature geothermal ORC systems. They pointed out that R123 and n-Pentane have better performance than PF5050, which had more preferable physical characteristics. Shu et al. [4] carried out an experimental comparison of R123 and R245fa for waste heat recovery from a heavy-duty diesel engine and obtained the result that R123 has an advantage at a heavy-duty level, while R245fa is more suitable for light-medium duty. Pang et al. [5] executed an experimental study on the organic Rankine cycle using R245fa, R123 and their mixtures, and obtained a maximum net power of 1.66 kW with their mixture (R245:R123, 2:1) as the working fluid. Wang et al. [6] investigated recovering engine waste heat and indicated that R11, R141b, R113 and R123 have slightly higher thermodynamic performance than the other considered fluids, while R245fa and R245ca are more environment-friendly than the others. Dai et al. [7] studied the cycle performance of several working fluids in an ORC system using a genetic algorithm and exergy analysis method. With a heat source temperature of 145 °C and an ambient temperature of 20 °C, R236ea has the highest exergy efficiency. Lakew et al. [8] screened several working fluids for ORC using different temperature heat sources and a theoretical method. R227ea gave the highest net power for ORC, using a 80–160 °C heat source, while R245fa gave the highest, using a 160–200 °C heat source. Though CO_2 is inorganic, it is still an important unconventional working fluid for positive cycles. Many researchers have studied the performance of a CO_2 trans-critical power cycle [9–13]. Zeotropic mixtures, composed of CO_2 and HCs, are also used for investigating the trans-critical power cycle [14,15]. Pan et al. paid a great deal of attention to the judgement of the pinch point position in exchangers for the ORC [16] and improved the conventional theoretical method for the ORC, based on the radial flow turbine, and gave the performance of several fluids for an ORC using 90 °C hot water as the heat source [17]. Researchers also took note of transient behavior in a system with an unstable source and have carried out much work in that regard [18–21].

The expansion component is the core of an ORC system. Wang et al. [22,23] established an ORC system integrated with a rolling rotor expander driven by solar energy. The expander gives a maximum isentropic efficiency of 45.2% and a maximum power of 1.73 kW with R245fa as the working fluid. Pan et al. [24] also tested a rolling rotor expander using CO_2 and obtained a maximum power generation of 1.7 kW. Gu [25] studied the performance of a small-scale ORC system that was integrated with a scroll expander and investigated the operational characteristics of the scroll expander. In the experimental study, the maximum electrical power of 1.1 kW is obtained using 80–100 °C hot water as the heat source. Guo [26] also carried out an experimental study on a scroll expander using 90 °C hot water as a heat source and obtained a maximum isentropic efficiency of 57.9%. Zhou et al. [27] fixed a scroll expander on an ORC system using 215 °C flue gas as a heat source, and they obtained a maximum output power of 645 W. Quoilin et al. [28] presented a numerical model and carried out an experimental study for an ORC system using a scroll expander. Declaye et al. [29] studied an open-drive scroll expander which was fixed to an ORC system, with R245fa as the working fluid. The maximum isentropic efficiency and shaft power could reach up to 75.7% and 2.1 kW, respectively. The maximum cycle efficiency of 8.5% was reached with evaporating temperature and condensing temperatures of 97.5°C and 26.6°C, respectively.

Expanders like piston expanders, scroll expanders and screw expanders are usually used in experimental ORC systems or in small heat capacity applications. A radial flow turbine is more practical for ORCs, rather than a volume type expander or axial turbine. A radial flow turbine has high efficiency for a low volume flow rate and high pressure ratio [30]. Rotational speed is usually very high in a radial flow turbine, which leads to a small turbine size and consequently a low initial investment. Fiaschi et al. [31] pointed out that the selection of the working fluid has relevant effects, both on cycle thermodynamics and on turbine efficiency. Pei et al. [32] established a solar driving ORC system that was integrated with a micro radial flow turbine, whose isentropic efficiency could reach

up to 65% when using R123 as the working fluid. Kang [33] designed an experimental system that integrated with a radial flow turbine and a high-speed generator and studied the system performance with R245fa as the working fluid. Three electric power values, 24.5 kW, 26.9 kW and 31.2 kW, were obtained correspondingly when the average evaporating temperature was 77.1, 79.5 and 82.3 °C, respectively. A tesla turbine is also a good choice for ORC applications [34,35].

Though many studies have been carried out on radial flow turbines, few researchers pay attention to the relationship between turbine performance and the operation parameters, as well as nozzle performance in the turbine. In this article, an experimental study is carried out on a small-scale ORC system which is integrated with a micro radial flow turbine to study the relationship between cycle performances and operation parameters. Cycle performances, such as specific energy ($\dot{P}_{specific}$, electrical power generated per unit mass flow rate of heat source fluid), thermal efficiency, turbine isentropic efficiency and transmission-generation efficiency are investigated and their variation trends with evaporating pressure and condensing pressure are obtained and analyzed in detail.

2. Methodology

2.1. The ORC System and the Micro Radial Flow Turbine

Figure 1 shows a scheme diagram of the ORC with R245fa as the working fluid. It is indicated that the slope of the saturated vapor line in the T-s diagram is positive for R245fa, which is similar with R123. It is known that a large amount of working fluid must be overheated before flowing into turbine to avoid the liquid hammer phenomenon. With such a slope of the saturated vapor line, the saturated vapor can be used to drive the turbine without overheating. However, a low superheat degree is needed to guard against fluctuation of the working conditions. In addition, an appropriate superheat degree at the turbine entrance leads to a reduction of the mean temperature difference between the hot water and the working fluid, with an associated decrease of exergy loss within the heat exchanger. It is worth noting that the pinch point is located at state point 6 for the evaporator and state point 3 for the condenser. The experimental system included three loops, namely the organic fluid loop, the hot water loop and the cooling water loop, as shown in Figure 2. The hot water loop provides heat energy to the working fluid in the evaporator. The cooling water loop cools the working fluid in the condenser. In the organic fluid loop, the working fluid expands in the turbine consequently drives turbine. Then, low pressure fluid condenses in condenser. Liquid fluid is pumped by a pump and is heated in the evaporator.

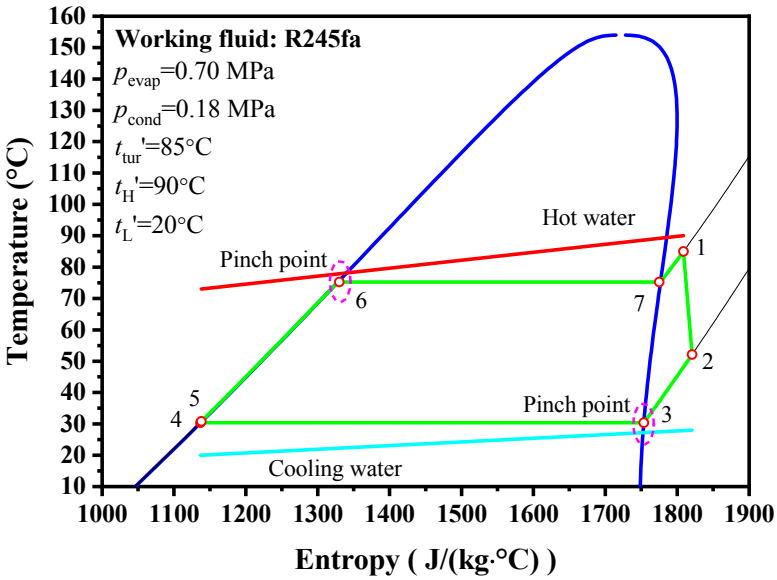

Figure 1. Scheme diagram of the organic Rankine cycle (ORC) (R245fa).

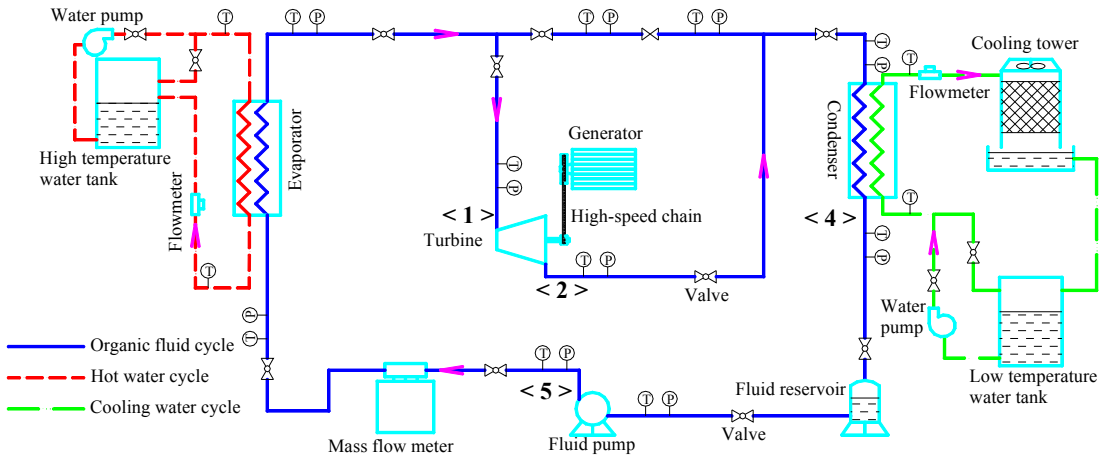

Figure 2. Flow chart of the ORC experimental system.

In the system, a micro radial flow turbine is used to convert heat energy to shaft work. As shown in Figure 3a, there are twelve prismatic blades, which share the same height and are fixed on the rotor. The rotor space is divided into twelve blade passages. Fluid flows toward the axis from the surrounding area and drives the rotor. There is only one position where the nozzle can be fixed, so it is a partial admission turbine. Two nozzle bases (the left is used) and two nozzle heads were manufactured for the turbine, as shown in Figure 3b. When the nozzle head is fixed on the nozzle base, a whole nozzle is prepared. In the experimental study, fluid states at the turbine entrance and turbine exit varied in different conditions, which caused variation in the turbine enthalpy drop. Consequently, fluid in the nozzle may need to expand at a subsonic speed in some conditions, while at a supersonic speed in other conditions. Then, a converging nozzle (with nozzle head I) and a Laval nozzle (with nozzle head II) were used. Using a Laval nozzle, a higher pressure drop can be obtained than with a converging nozzle under enough inlet pressure. There are several bends on the nozzle. Their role is to lead fluid flow towards the rotor. Details of the nozzle base used in the experimental investigation are shown in Figure 3c.

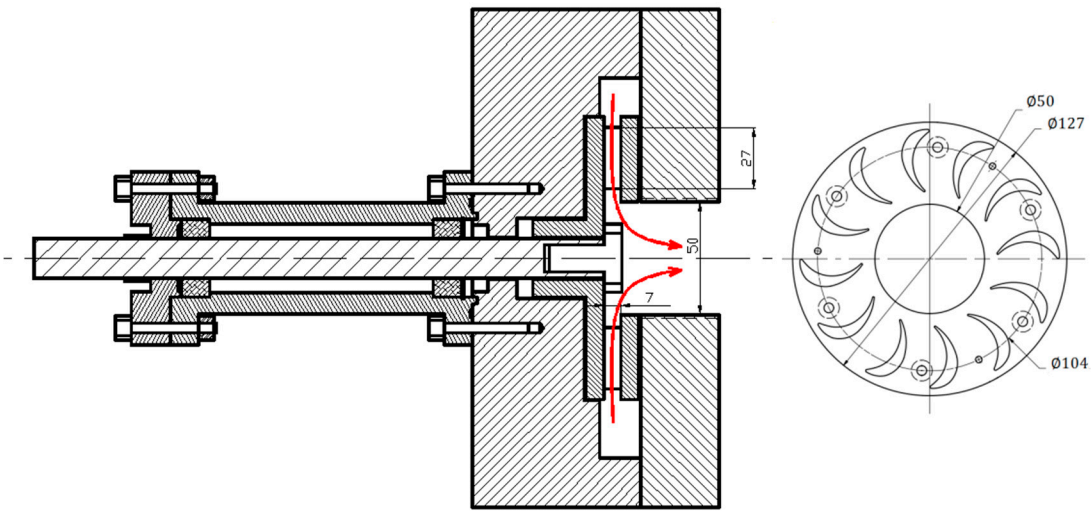

(**a**)

Figure 3. *Cont.*

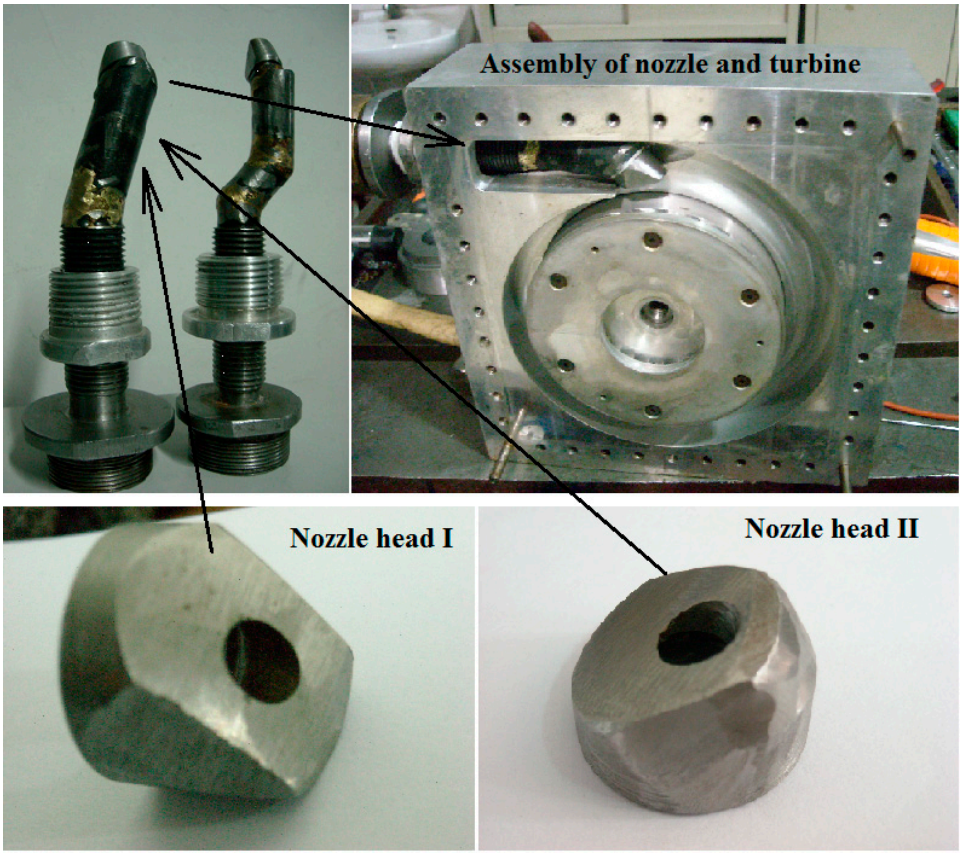

(**b**)

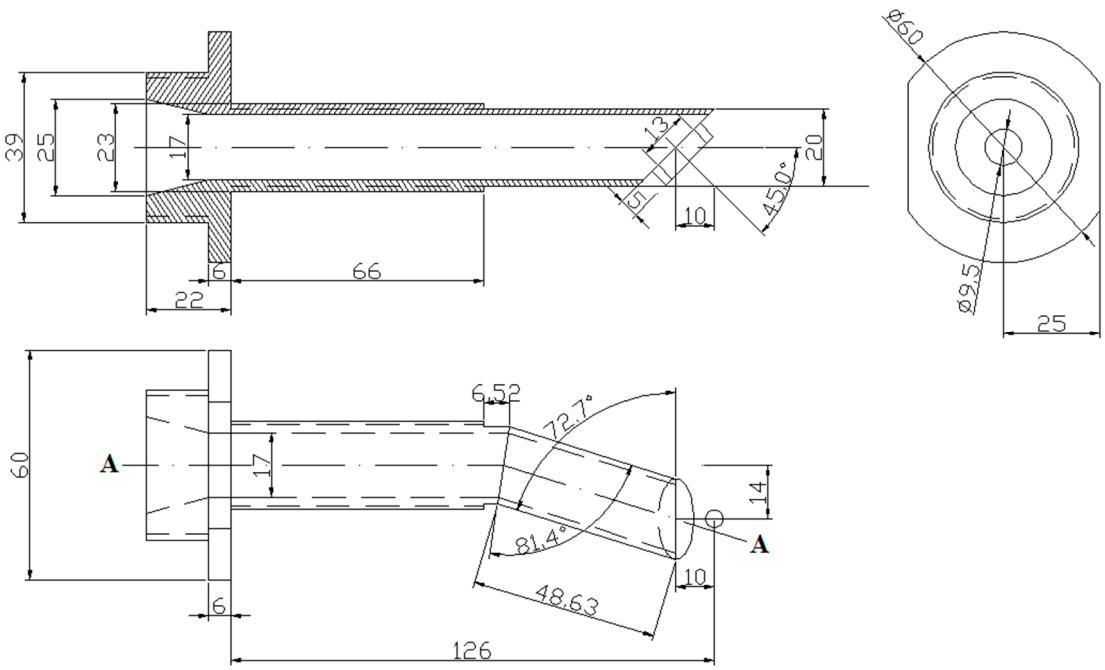

(**c**)

Figure 3. (**a**): Details of the radial flow turbine. (**b**): The assembly of the turbine nozzle. (**c**): Details of the nozzle without a nozzle head.

Adjustable resistance was used to consume the generated electricity. A slider that controlled the adjustable resistance was used to change the resistance value for different conditions. In a specified

condition, the resistance value of each phase must be approximately equal to make the turbine and generator rotate smoothly. The value of load resistance is closely related to generator speed and turbine speed. In stable conditions, the generator load torque is equal to the turbine torque. Generator load is mainly determined by load resistance and the turbine torque is impacted by the condition of the ORC. However, torque that is output from the turbine is not completely converted into electricity. There are several losses in the generator and in the transmission of torque from the turbine to the generator. Generator loss includes magnetic flux leakage loss, internal friction loss and internal coil heat loss. All the losses are considered as part of generator load torque. Therefore, the turbine speed can be regulated by changing the load resistance, turbine inlet state parameters and turbine outlet state parameters. In the experimental study, the ORC condition can be obtained by regulating the system parameters (mass flow rate of hot water, mass flow rate of cooling water and mass flow rate of working fluid, etc.) and a specified turbine speed can be obtained by regulating the load resistance.

There are some other instruments and devices in the system, such as the evaporator, condenser, fluid pump, cooling tower, mass flowmeter, data logger and power meter. Information of the main instruments and measuring devices is shown in Table 1.

Table 1. Information of instruments and measuring devices.

Item	Information
Evaporator	Two plate heat exchangers which are connected in series are used as evaporator of the ORC system. Evaporator-I: SWEP B10T × 20H/1P; 0.558 m^2 Evaporator-II: SWEP V200T × 60H/1P; 7.48 m^2
Condenser	A plate heat exchanger is used as condenser. The model number is SWEP B200T × 50H/1P. The area is 6.19 m^2.
Fluid pump	A hydraulic diaphragm metering pump is used in the system. The model number is SJ4-M-630/2.5. The rated flow is 630 L/h. The upper limit pressure is 2.5 MPa.
Generator	It is a permanent magnet generator. Starting torque is 1.2 N·m. Rated speed is 360 rpm. Rated power and rated voltage are 1.0 kW and 56 V (DC).
Cooling tower	The model number is DBNL3.
Mass flowmeter	Coriolis mass flowmeter is used in the system. The model number is DMF1-4. The measuring range is 0–2000 kg/h and the accuracy class is 0.2. The working pressure is 0–10 MPa.
Data logger	Agilent 34970A is used to log temperature, pressure and mass flow rate in the system.
Power meter	Model number of the digital power meter used in the experiment is WT230. Measuring range of voltage is 0–600 V and measuring range of electric current is 0–20 A. Applicable frequency range is 0 and 0.5–100 kHz. The accuracy in measuring power generated can be calculated by $\dot{P} \times 0.001 + \Delta\dot{P} \times 0.001$ where $\dot{P}$ represents the displayed value and $\Delta\dot{P}$ represents the measuring range selected.

Two organic fluids, namely R245fa and R123, were used in the experimental study. Both of them have zero or very little ozone depression potential (ODP). The basic thermal and environmental properties of the fluids are shown in Table 2.

Table 2. Basic thermal properties and environmental properties of considered fluids [36].

Substance	M	t_b	t_c	p_c	LFL	ASHRAE 34 Safety Group	Atmospheric Life	ODP	GWP
	g/mol	°C	°C	MPa	%		yr		100 yr
R245fa	134.05	15.14	154.01	3.651	none	B1	7.6	0	1030
R123	152.93	27.82	183.68	3.662	none	B1	1.3	0.02	77

2.2. Experimental Method

In the experimental study, several parameters were regulated by the researchers' own initiative, such as the working fluid, turbine speed, temperature of hot water, flow rate of hot water, temperature of cooling water and the mass flow rate of cooling water. The inverter that is fixed on the fluid pump is used to control the mass flow rate of the working fluid. The turbine speed depends on the ORC condition and load resistance. When the ORC condition is specified, the load resistance can be used to regulate the turbine speed. The temperature of the hot water is regulated by changing the heating electric power applied to the hot water. Temperature of the cooling water is regulated by changing the air flow rate in the cooling tower. The flow rates of the hot water and cooling water are regulated by adjusting the main valves and bypass valves.

The turbine inlet pressure can be regulated by changing the fluid mass flow rate. The degree of superheat in the turbine entrance can be regulated by the changing temperature and mass flow rate of the hot water. Additionally, the evaporating pressure will also be influenced by this method. The degree of subcooling and condensing pressure can be regulated by changing the temperature and mass flow rate of the cooling water.

2.3. Definition of Performance Parameters

Fluid expands in the turbine and drives the rotor. Because of losses in the turbine nozzle and turbine blade passages, the real enthalpy drop is lower than the isentropic enthalpy drop. It is worth noting that the kinetic energy is not considered in order to simplify the analysis, so enthalpy is equal to the total enthalpy at each state point. Turbine isentropic efficiency is defined as the ratio of the real enthalpy drop to the isentropic enthalpy drop, and can be expressed as follows:

$$\eta_{\text{tur,isen}} = \frac{h_1 - h_2}{h_1 - h_{2,\text{isen}}} \tag{1}$$

A high-speed chain was used to transmit torque from the turbine shaft to the generator shaft. There were losses in torque transmission and electricity generation. Torque transmission loss is mechanical loss that occurred in the turbine, high-speed chain and generator. The electricity generation loss that occurred in the generator mainly includes coil loss and magnetic flux leakage loss, which are determined by the generator speed and load resistance. In the experimental study, it was difficult to separate the transmission loss and generation loss, so a performance parameter named transmission-generation efficiency was defined and can be calculated by Equation (2).

$$\eta_{\text{trans-ge}} = \frac{\dot{P}_{\text{ge}}}{\dot{m}_{\text{fluid}}(h_1 - h_2)} \tag{2}$$

The evaporator heat transfer rate can be expressed by Equation (3). In a theoretical study on ORC performance, thermal efficiency is usually defined as the ratio of the net power output to the evaporator heat transfer rate. In small-scale experimental systems, the actual capacity of equipment usually does not match perfectly and the actual efficiencies of the turbine and pump are usually very low, which leads the pump usually consuming as much electrical power as the whole system outputs. In an actual large-scale project, the turbine incontrovertibly outputs a much greater amount of power than the pump consumes. The role of the experimental system is to obtain some scientific laws for the working fluid, cycle or system. Therefore, if defined as the ratio of net power output to evaporator heat transfer rate, thermal efficiency becomes meaningless in an experimental study on a small-scale ORC system. In this article, thermal efficiency is defined as the ratio of electrical power generated to the evaporator heat transfer rate, and can be expressed by Equation (4).

$$\dot{Q}_{\text{evap}} = \dot{m}_{\text{fluid}}(h_1 - h_5), \tag{3}$$

$$\eta_{\text{ther}} = \frac{\dot{P}_{\text{ge}}}{\dot{Q}_{\text{evap}}}, \tag{4}$$

In most cases, the mass flow rate of the heat source fluid, like water and gas, is constant, so the electrical power generated per unit of mass flow rate of heat source fluid is usually selected as an objective function. Here, the specific energy ($\dot{P}_{\text{specific}}$) is defined as the ratio of electrical power generated to the mass flow rate of the hot water and can be expressed as below:

$$\dot{P}_{\text{specific}} = \frac{\dot{P}_{\text{ge}}}{\dot{m}_{\text{hot water}}} \tag{5}$$

The unit of electrical power is the kW and unit of the mass flow rate of the hot water is kg/s. This means that the unit of specific energy is $\text{kJ}_{(\text{electrical energy})}/\text{kg}_{(\text{hot water})}$. Therefore, $\dot{P}_{\text{specific}}$ also represents the electrical energy that can be exploited from the unit mass of the hot water. A typical parameter for characterizing turbine performance is the isentropic velocity ratio, which is expressed as follows:

$$x_{\text{tur,isen}} = \frac{u_{\text{tur}}}{\sqrt{2(h_1 - h_{2\text{s}})}} \tag{6}$$

2.4. Uncertainty of Experimental Data

The uncertainty of experimental results is impacted by the accuracy of equipment, measurement error and so on. In this article, only the uncertainty of equipment is considered. Temperature was measured by a T-type thermocouple which had an accuracy of 0.5 °C. The system must be vacuumed before being filled with the working fluid. Therefore, pressure gauges (including the vacuum range) are used to measure the pressure in the system. The accuracy of the pressure gauges is 0.001 MPa. The measuring accuracy of the working fluid mass flow rate and water volume flow rate are 0.001 kg/s and 0.0625 L/s, respectively. Accuracy in measuring the generated power can be calculated by $\dot{P} \times 0.001 + \Delta\dot{P} \times 0.001$, where $\dot{P}$ represents the displayed value and $\Delta\dot{P}$ represents the selected measuring range. Errors that arise from heat loss to the environment and the properties of working fluid are neglected.

The uncertainty of parameters measured by the equipment directly are not shown in the result figures, while that of the derived parameters is shown in the figures. From definitions of $\eta_{\text{tur,isen}}$, $\eta_{\text{trans-ge}}$ and $\dot{Q}_{\text{evap}}$, their uncertainties can be expressed as follows:

$$U_{\eta,\text{tur,isen}} = \sqrt{\left(U_{\text{h},1}\frac{\partial\eta_{\text{tur,isen}}}{\partial h_1}\right)^2 + \left(U_{\text{h},2}\frac{\partial\eta_{\text{tur,isen}}}{\partial h_2}\right)^2 + \left(U_{\text{h},2,\text{isen}}\frac{\partial\eta_{\text{tur,isen}}}{\partial h_{2,\text{isen}}}\right)^2} \tag{7}$$

$$U_{\eta,\text{trans-ge}} = \sqrt{\left(U_{\dot{\text{P}},\text{ge}}\frac{\partial\eta_{\text{trans-ge}}}{\partial\dot{P}_{\text{ge}}}\right)^2 + \left(U_{\dot{\text{m}},\text{fluid}}\frac{\partial\eta_{\text{trans-ge}}}{\partial\dot{m}_{\text{fluid}}}\right)^2 + \left(U_{\text{h},1}\frac{\partial\eta_{\text{trans-ge}}}{\partial h_1}\right)^2 + \left(U_{\text{h},2}\frac{\partial\eta_{\text{trans-ge}}}{\partial h_2}\right)^2} \tag{8}$$

$$U_{\text{Q,evap}} = \sqrt{\left(U_{\text{m,fluid}}\frac{\partial\dot{Q}_{\text{evap}}}{\partial\dot{m}_{\text{fluid}}}\right)^2 + \left(U_{\text{h},1}\frac{\partial\dot{Q}_{\text{evap}}}{\partial h_1}\right)^2 + \left(U_{\text{h},5}\frac{\partial\dot{Q}_{\text{evap}}}{\partial h_5}\right)^2} \tag{9}$$

In the above equations, the enthalpy value of the working fluid was obtained from the Reference Fluid Thermodynamic and Transport Properties (REFPROP) [37] by inputting the pressure and temperature. The relationship between enthalpy, pressure and temperature can be expressed as in Equation (10), so the uncertainty of enthalpy can be calculated by Equation (11). The values of c_{p} and $\left(\frac{\partial v}{\partial t}\right)_{\text{p}}$ were also obtained from REFPROP.

$$dh = c_p \mathrm{d}t + \left[v - t\left(\frac{\partial v}{\partial t}\right)_p \right] \mathrm{d}p \tag{10}$$

$$U_h = \sqrt{\left(U_{t,fluid}\frac{\partial h}{\partial t_{fluid}}\right)^2 + \left(U_{p,fluid}\frac{\partial h}{\partial p_{fluid}}\right)^2} \tag{11}$$

The uncertainties of η_{ther} and $\dot{P}_{specific}$ can be derived from Equations (4) and (5), as shown in the following equations:

$$U_{\eta,ther} = \sqrt{\left(U_{\dot{P},ge}\frac{\partial \eta_{ther}}{\partial \dot{P}_{ge}}\right)^2 + \left(U_{\dot{Q},evap}\frac{\partial \eta_{ther}}{\partial \dot{Q}_{evap}}\right)^2} \tag{12}$$

$$U_{\dot{P},specific} = \sqrt{\left(U_{\dot{P},ge}\frac{\partial \dot{P}_{specific}}{\partial \dot{P}_{ge}}\right)^2 + \left(U_{\dot{m},hot\ water}\frac{\partial \dot{P}_{specific}}{\partial \dot{m}_{hot\ water}}\right)^2} \tag{13}$$

According to Equation (6), the isentropic velocity ratio of the turbine can be expressed as below:

$$U_{x,tur,isen} = \sqrt{\left(U_{u,tur}\frac{\partial x_{tur,isen}}{\partial u_{tur}}\right)^2 + \left(U_{h,1}\frac{\partial x_{tur,isen}}{\partial h_1}\right)^2 + \left(U_{h,2}\frac{\partial x_{tur,isen}}{\partial h_{2s}}\right)^2} \tag{14}$$

3. Results and Discussion

3.1. Performance versus Evaporating Pressure with Constant Condensing Pressure

In this section, system performances such as the outlet temperature of hot water, the mass flow rate of fluid, the evaporator heat transfer rate, the turbine isentropic efficiency, the transmission-generation efficiency, the specific energy and thermal efficiency are investigated. The system operating parameters were controlled according to Table 3.

Table 3. Parameters range in experiment.

Fluids	$t_{hot\ water}'$	$t_{cooling\ water}'$	t_{tur}'	n_{tur}	p_{cond}	t_{cond}	p_{evap}	t_{evap}
	°C	°C	°C	rpm	MPa	°C	MPa	°C
R245fa	90	20	85	4200	0.180	30.5	0.40–0.70	55–75
R123	90	20	85	4200	0.110	30.0	0.30–0.50	61.7–80.9

As shown in Figure 4a, in both experimental series, the outlet temperature of the hot water increased with the increase of evaporating pressure. The mass flow rate of the hot water and the evaporator heat transfer rate increased with increasing evaporating pressure. In order to increase the evaporating pressure, the mass flow rate of working fluid was enhanced, meaning a larger evaporator heat transfer rate was required. Therefore, the mass flow rate of hot water increases with the rise of evaporating pressure. The outlet temperature of the hot water was determined by the pinch point temperature difference and the evaporating temperature. When the pinch point temperature difference remained constant, the water outlet temperature increased with rising evaporating pressure. As shown in Figure 4a, the evaporator heat transfer rate with nozzle I is nearly equal to that of nozzle II, while the outlet temperature of the hot water and the mass flow rate of the hot water with nozzle I are very different from that with nozzle II. The reason for this is that the pinch point temperature differences in both experimental series are different from each other. The pinch point temperature difference with nozzle I is lower than that with nozzle II, so the water outlet temperature with nozzle I is obviously

lower than that of nozzle II. The equality of the evaporator heat transfer rate and the higher water outlet temperature lead to a higher mass flow rate of hot water.

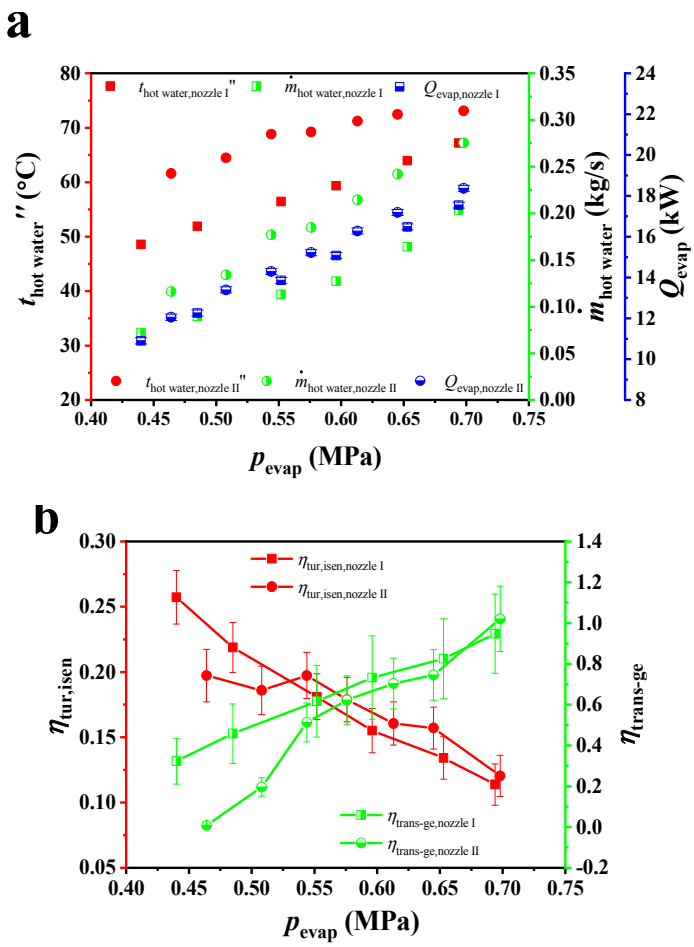

Figure 4. Variation of system performance with evaporating pressure (R245fa). (**a**): Parameters about the hot water; (**b**): Efficiency about the turbine and the generator.

As shown in Figure 4b, in both experimental series, turbine isentropic efficiency decreased with increasing evaporating pressure, while transmission-generation efficiency increased with the increase of evaporating pressure. Axis clearance leakage in the turbine rose with the increase of turbine inlet pressure, which leads to a decrease in turbine isentropic efficiency with the increase of turbine inlet pressure. When the turbine speed and generator speed were kept constant, the generator efficiency increased with the decrease of load resistance [38]. The load resistance decreased with the rise of evaporating pressure, so the transmission-generation efficiency increases with the increase of evaporating pressure.

It is also shown in Figure 4b that the turbine isentropic efficiency with nozzle I was higher than that of nozzle II in conditions with low evaporating pressure, while the turbine isentropic efficiency of nozzle I was lower than that of nozzle II in conditions with high evaporating pressure conditions. When the evaporating pressure is low there may be shock loss in the Laval nozzle, and shock loss decreases with rising evaporating pressure.

Figure 5 shows the expansion process in the converging nozzle and Laval nozzle [39]. If the back pressure was equal to the design value at the exit of converging nozzle, the working fluid expanded from the inlet pressure to the design pressure (or backpressure), which is represented by the line AC. If the back pressure was higher than the design value, the fluid expanded to the back pressure, which is represented by the line AB. However, if the back pressure was lower than the design value, the

fluid expanded to the design pressure in the converging nozzle and its pressure quickly decreased to the back pressure along line ACD. The expansion process, represented by line ACD, is also known as underexpansion. The expansion process in the Laval nozzle is more complicated than that of the converging nozzle. Undoubtedly, if the back pressure is equal to design value at the exit of Laval nozzle, the working fluid expands from the inlet pressure to the design pressure (or back pressure) along line AC. If the back pressure is lower than the design value, underexpansion also occurs along line ACD. It is worth noting that overexpansion occurs in the Laval nozzle when the back pressure is higher than the design value. In the expansion section of the Laval nozzle, a supersonic expansion velocity was achieved, and a shockwave was generated at the cross section (point E) where the fluid pressure jumps to a higher value and the fluid velocity decreases to a subsonic (dotted line EF) level. Then, the fluid is compressed in the remaining expansion section and reaches back pressure at the exit. The cross section moves to the throat with rising back pressure. Line AMN shows the expansion process in which the shockwave occurs at the throat. This shockwave, which is irreversible and causes kinetic energy loss, should be avoided as much as possible.

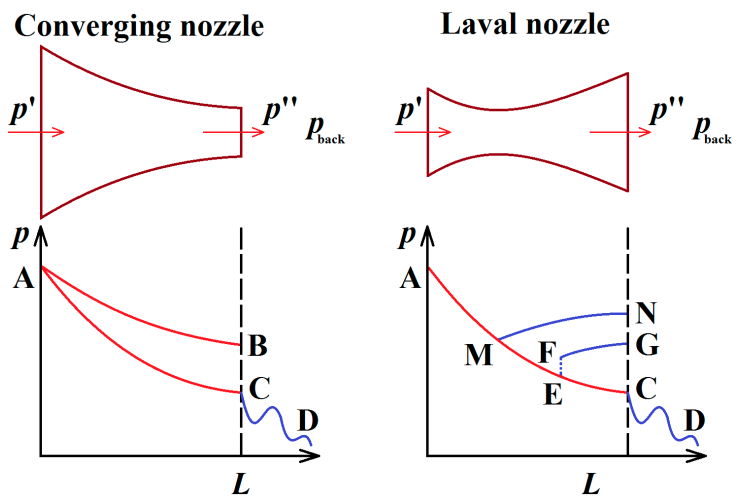

Figure 5. Expansion process in nozzle.

When the evaporating pressure is high, leakage loss is the main loss in the turbine when using a converging nozzle. Therefore, a converging nozzle is suitable for low inlet pressure while a Laval nozzle is more suitable for high inlet pressure in the considered turbine. When the evaporating pressure was high, the transmission-efficiency was nearly the same in both experimental series. When evaporating pressure was low, the turbine torque with nozzle II was low, which lead to large load resistance. Therefore, the transmission-generation efficiency with nozzle II is lower than of nozzle I. It should be noted that the transmission-generation efficiency value which is indirectly obtained from the experimental data is sometimes a little higher than 1.0. This is a result of measurement error of turbine inlet pressure, turbine inlet temperature and generated power.

As shown in Figure 6, variation of the considered parameters and the performance with R123 as working fluid was similar to that with R245fa as working fluid. As shown in Figure 6a, the water outlet temperature and mass flow rate of the hot water in both experimental series are coincident. The reason for this is that the pinch point temperature difference in both experimental series may be equal. The pinch point in an evaporator for a subcritical ORC is usually located at the bubble point. At a specified evaporating pressure, the outlet temperature of hot water is equal for experiment with nozzle I and nozzle II. As indicated in Figure 1, the pinch point temperature difference between both experimental series is equal.

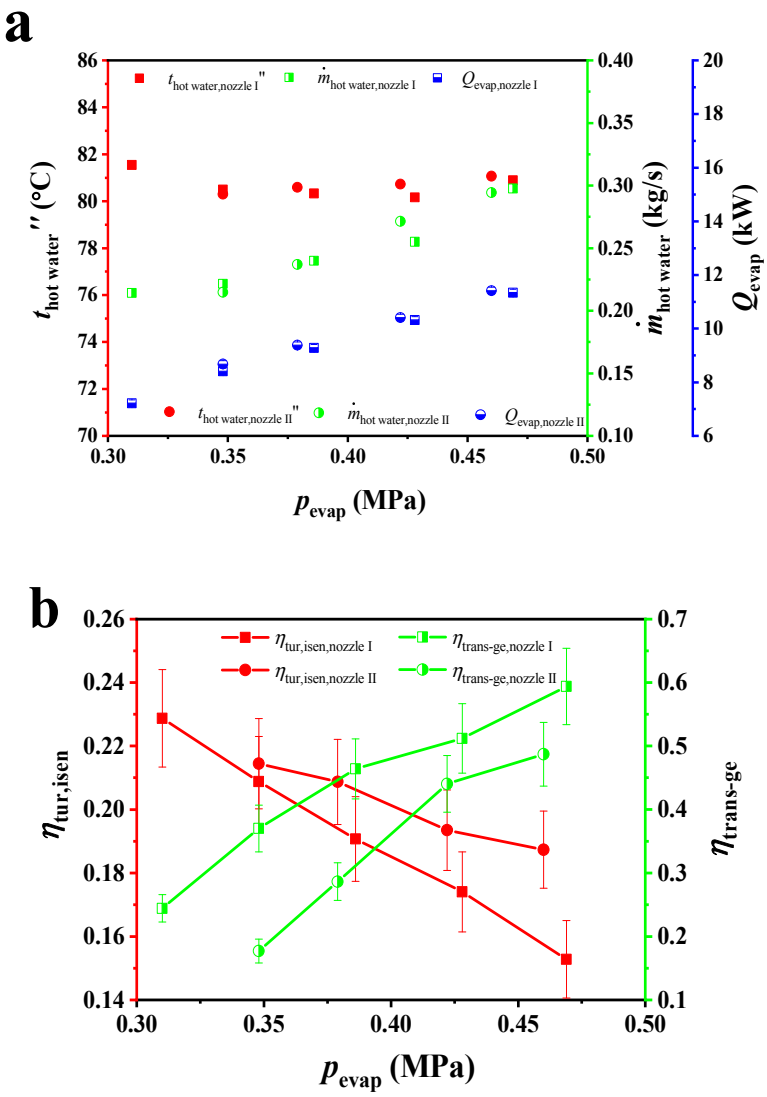

Figure 6. Variation of system performance with evaporating pressure (R123). (**a**): Parameters about the hot water; (**b**): Efficiency about the turbine and the generator.

As shown in Figure 7, when R245fa was selected as a working fluid, the specific energy increased firstly and then decreased with the rise of evaporating temperature. With nozzle I, the maximum specific energy was 1.28 kJ/kg and the optimal evaporating temperature was 69.2 °C. With nozzle II, the maximum specific energy was 0.87 kJ/kg and the optimal evaporating temperature was 75.2 °C. When R123 was used as the working fluid, the specific energy increased with increasing evaporating temperature and the maximum value may appear in conditions with higher evaporating temperatures. The maximum specific energy was 0.39 kJ/kg with nozzle I and 0.40 kJ/kg with nozzle II.

Thermal efficiency (as shown in Figure 8) and water outlet temperature (as shown in Figure 6a) increased with rising evaporating temperature. Specific energy increased with the increase of thermal efficiency and decreased with the increase of water outlet temperature. Therefore, specific energy increases firstly and then decreases with the rise of evaporating temperature. In addition, transmission-generation efficiency increases with increasing evaporating temperature.

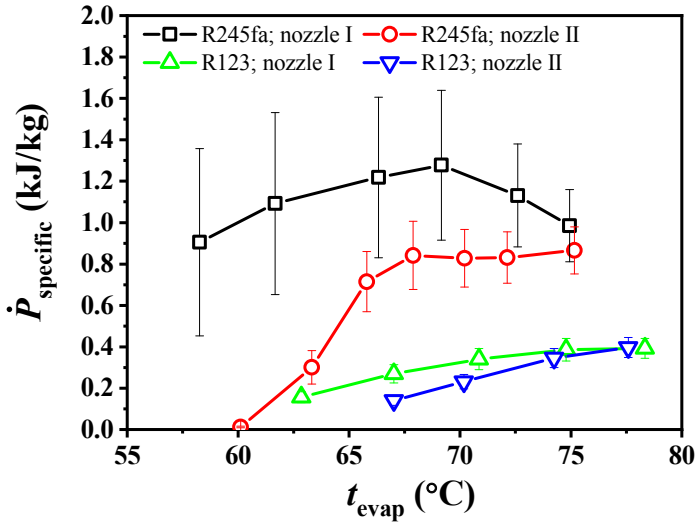

Figure 7. Variation of specific energy with evaporating temperature.

As shown in Figure 8, the thermal efficiency increased with the increase of evaporating temperature. When the turbine inlet temperature is kept constant, the thermal efficiency is mainly determined by the evaporating and condensing temperatures. In the experiment, the condensing temperature was kept at approximately 30 °C, so the thermal efficiency increased with the increase of evaporating temperature.

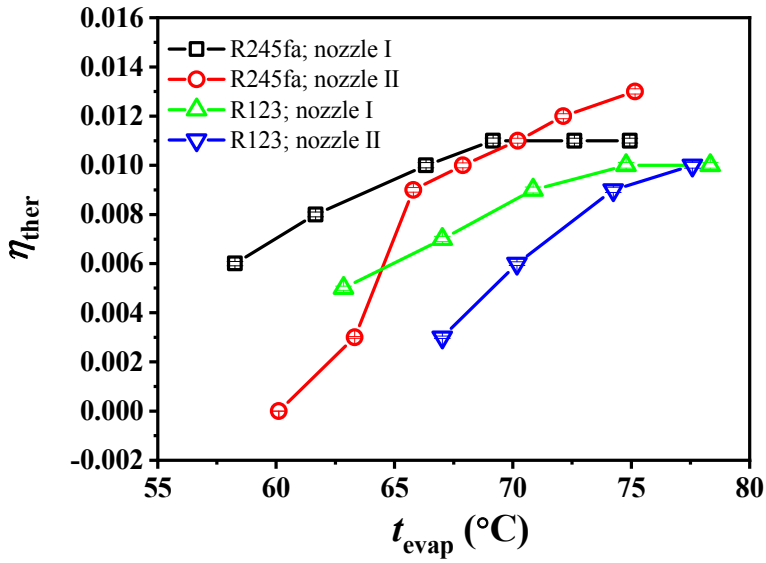

Figure 8. Variation of thermal efficiency with evaporating temperature.

3.2. Performance versus Condensing Pressure with Constant Evaporating Pressure

In this section, several system performances are investigated, and the system operating parameters were controlled according to Table 4.

Table 4. Parameters range in experiment.

Fluids	$t_{hot\ water}'$	$t_{cooling\ water}'$	t_{tur}'	n_{tur}	p_{evap}	t_{evap}	p_{cond}	t_{cond}
	°C	°C	°C	rpm	MPa	°C	MPa	°C
R245fa	90	20	85	4200	0.690	75.0	0.170–0.300	28.7–45.6
R123	90	20	85	4200	0.440	75.9	0.100–0.200	27.5–48.0

Figure 9a shows that the outlet temperature of the cooling water increased with the increase of condensing pressure and mass flow rate of cooling water decreased with the rise of condensing pressure. Variation of the outlet temperature of the cooling water and the mass flow rate of the cooling water in both experimental series is coincidental. The outlet temperature of the cooling water increased with the increase of condensing pressure when the inlet temperature of the cooling water and the pinch point temperature difference of condenser were kept constant. In the considered conditions, the mass flow rate of the working fluid nearly was kept constant, so the mass flow rate of the cooling water decreased with the increase of condensing pressure and outlet temperature of the cooling water.

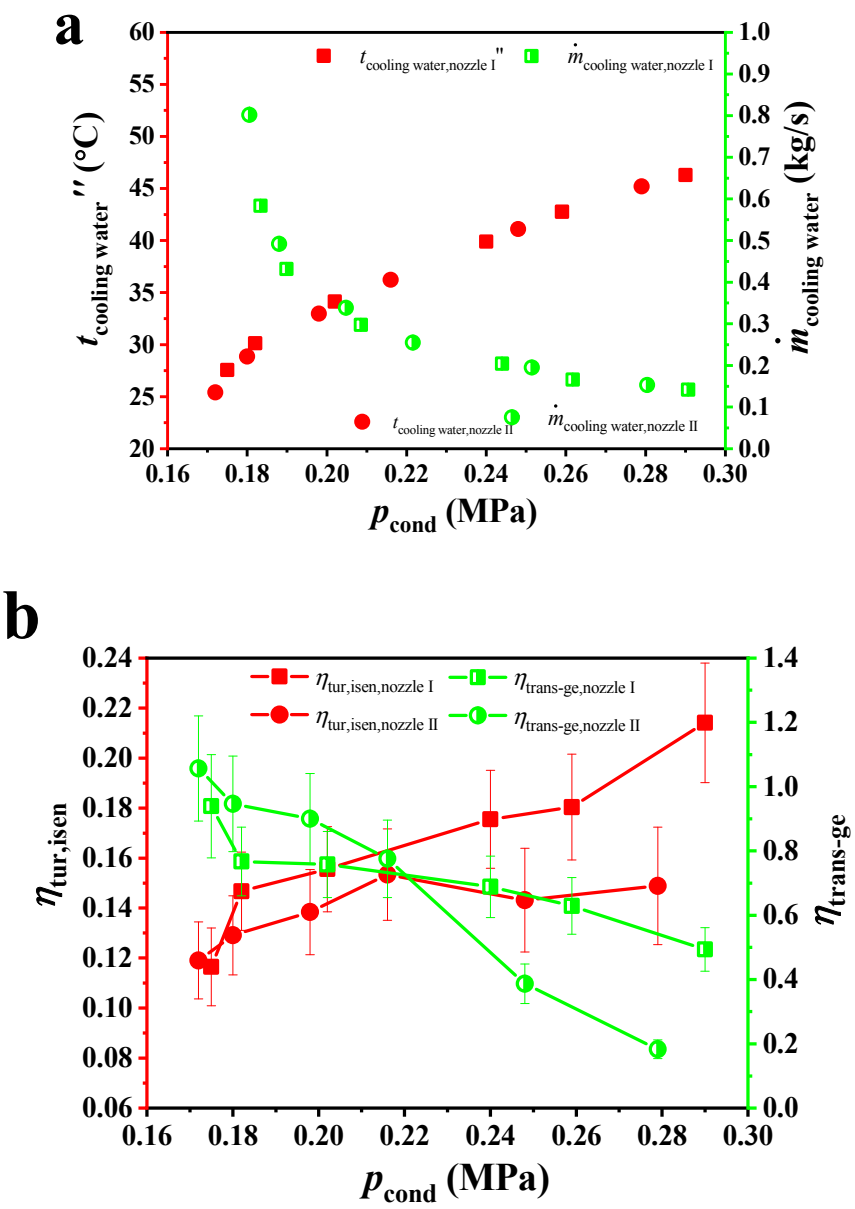

Figure 9. Variation of system performance with condensing pressure (R245fa). (**a**): Parameters about the cooling water; (**b**): Efficiency about the turbine and the generator.

As shown in Figure 9b, the turbine isentropic efficiency increased with the increase of condensing pressure, while transmission-generation efficiency decreased with rising condensing pressure. With nozzle I, the differential pressure and leakage loss decreased with the increase of condensing pressure. Therefore, turbine isentropic efficiency increases rapidly with the increase of condensing pressure. With nozzle II, differential pressure and leakage loss decreased with the increase of

condensing pressure, while shock loss increased with the increase of condensing pressure. Therefore, turbine isentropic efficiency increased slightly with nozzle II. Turbine torque decreased with the increase of condensing pressure. When the turbine speed was kept constant, the load resistance increased with the increase of condensing pressure. Therefore, transmission-generation efficiency decreased with the increase of condensing pressure.

As shown in Figure 10, the variation of the considered parameters and performance with R123 as working fluid was similar when R245fa was used as the working fluid.

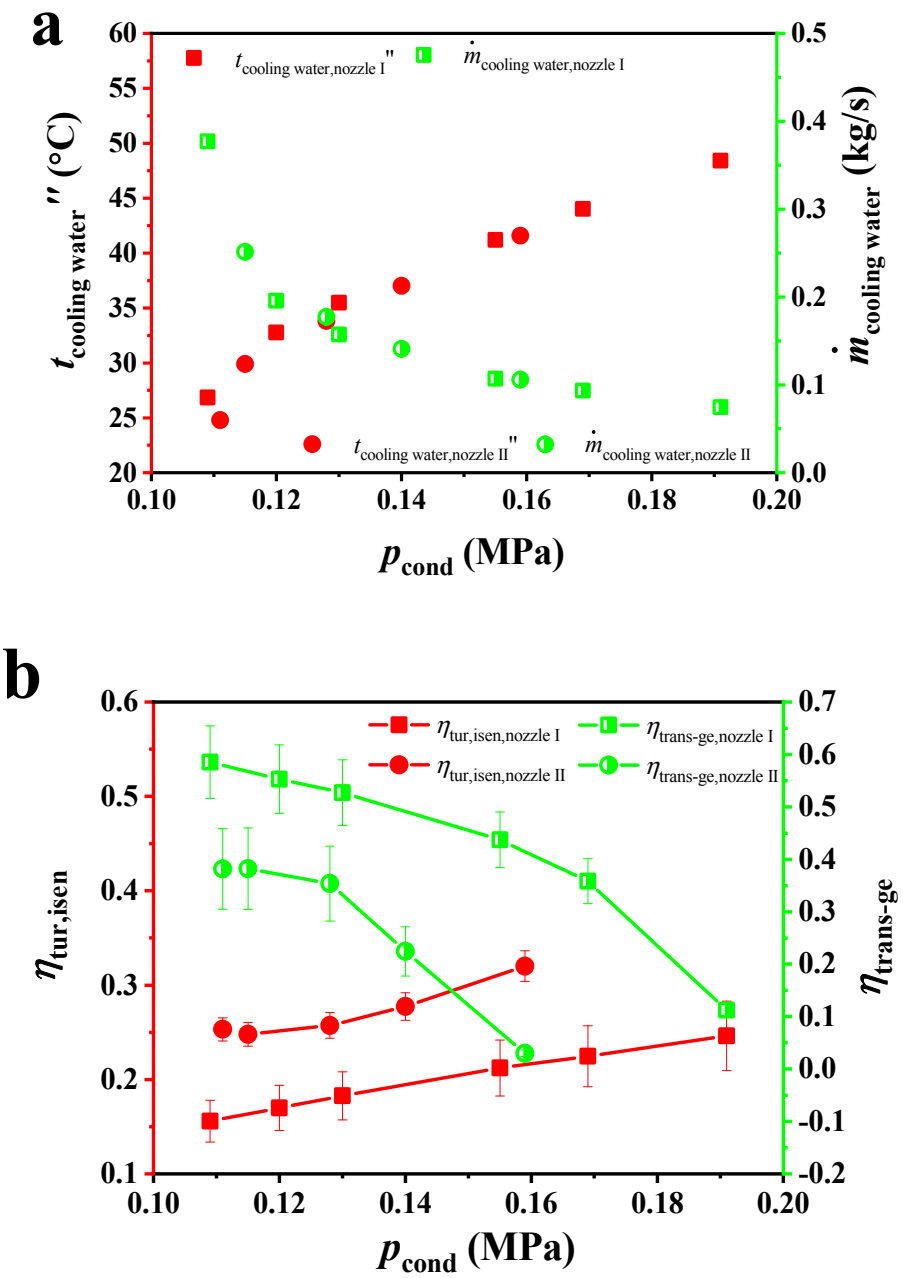

Figure 10. Variation of system performance with condensing pressure (R123). (**a**): Parameters about the cooling water; (**b**): Efficiency about the turbine and the generator

As shown in Figure 11, the specific energy decreased with the increase of condensing temperature. There may be maximum value of specific energy at lower condensing temperatures. However, an experiment with lower condensing temperature was not carried out because the temperature of the cooling water was not low enough.

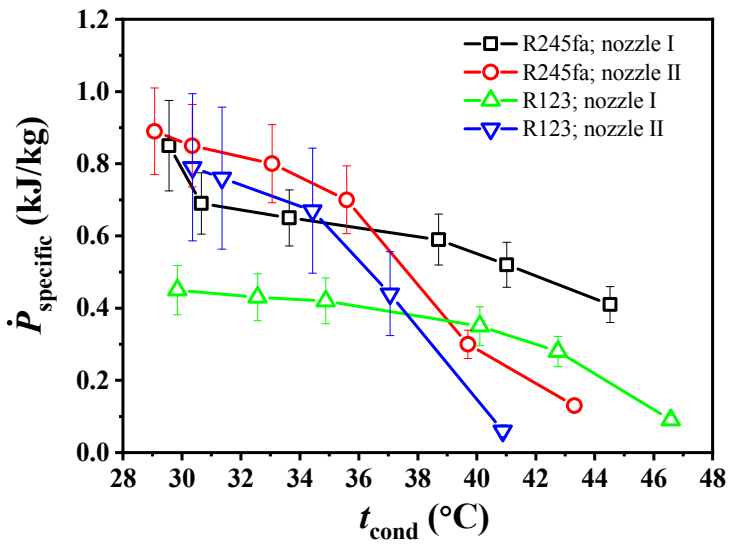

Figure 11. Variation of specific energy with condensing temperature.

When R245fa was selected as the working fluid, the maximum specific energy was 0.69 kJ/kg with a condensing temperature of 30.7 °C with nozzle I and 0.89 kJ/kg with a condensing temperature of 29.1 °C with nozzle II. When R123 was selected as the working fluid, the maximum specific energy was 0.45 kJ/kg with a condensing temperature of 29.9 °C with nozzle I and 0.79 kJ/kg with a condensing temperature of 30.4 °C with nozzle II. When the evaporating temperature was constant, the turbine inlet pressure was constant. The turbine outlet pressure increased with the increase of condensing temperature. Therefore, the pressure drop decreased with the increase of condensing temperature, which lead to the decrease in specific energy.

As shown in Figure 12, thermal efficiency decreased with the increase of condensing temperature. Thermal efficiency is determined by the evaporating temperature and condensing temperature. When the evaporating temperature was kept constant, thermal efficiency decreased with increasing condensing temperature.

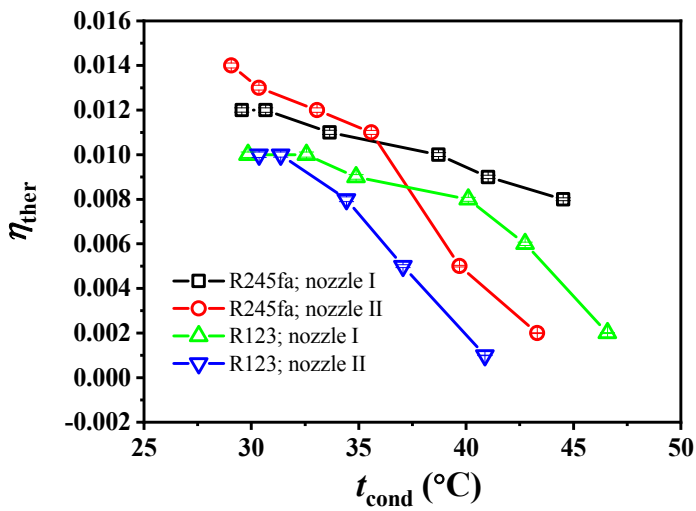

Figure 12. Variation of thermal efficiency with condensing temperature.

3.3. Turbine Performance vs. Isentropic Velocity Ratio

In order to analyze the turbine performance, the relationship between turbine isentropic efficiency and the turbine isentropic velocity ratio is shown in Figure 13, according to the above experimental data. Generally speaking, turbine isentropic efficiency increased with a rising isentropic velocity ratio,

but the peak value did not appear in the considered conditions. The maximum value may be obtained with a higher isentropic velocity ratio, which cannot be reached using the current experimental system. Therefore, a low isentropic velocity ratio was a main reason for such a low isentropic efficiency, besides partial admission, leakage loss, shock loss, incidence loss and so on. In addition, the turbine with nozzle I ran more stably with varied conditions and working fluids. The reason for this is that the converging nozzle is more adaptable to varied back pressure than the Laval nozzle, whose performance is seriously impacted by shock loss.

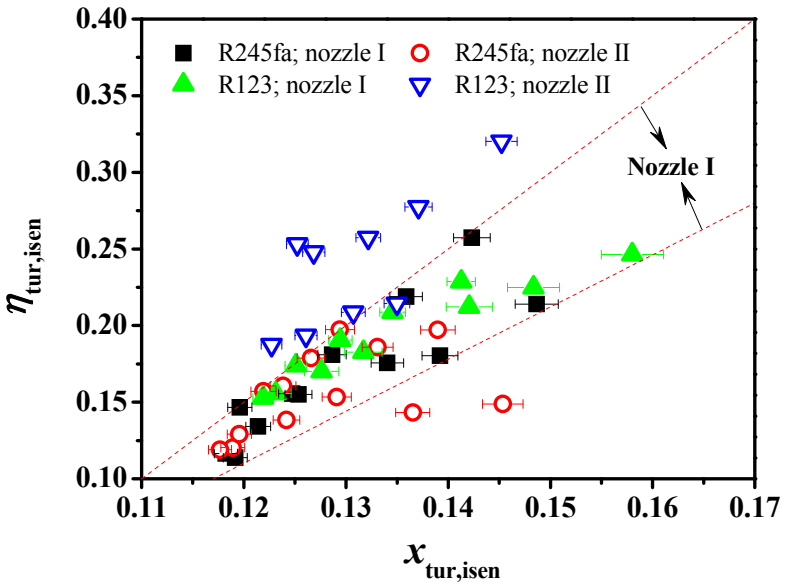

Figure 13. Variation of turbine isentropic efficiency with isentropic velocity ratio.

4. Conclusions

In a small-scale ORC experimental system, this article studied the relationship between cycle performances and operation parameters, especially when achieved by varying the turbine performance and nozzle performance with evaporating pressure and condensing pressure.

(1) With constant condensing pressure (temperature), turbine isentropic efficiency decreased, and transmission-generation efficiency increased with increasing evaporating pressure. The specific energy of R245fa showed a peak of 1.28 kJ/kg with an evaporating temperature of 69.2 °C. Specific energy increased monotonously with rising evaporating temperature for R123.

(2) With constant evaporating pressure (temperature), the turbine isentropic efficiency increased, and transmission-generation efficiency decreased with rising condensing pressure. The specific energy for both working fluids decreased with increasing condensing temperature in the considered conditions. The maximum specific energy was 0.89 kJ/kg with the optimal fluid (R245fa) and an optimal condensing temperature of 29.1 °C.

(3) Turbine efficiency was impacted by the working fluid type, operation parameters and nozzle type.

Author Contributions: Conceptualization, H.W.; Data curation, L.P.; Methodology, L.P.

Funding: Projects 51376134 and 51306198, supported by National Natural Science Foundation of China, are gratefully acknowledged.

Conflicts of Interest: The authors declare no conflict of interest.

Nomenclature

M	molar mass (g/mol)
p	pressure (MPa)
t	temperature (°C)
c	specific heat capacity (kJ/(kg·°C))
h	enthalpy (kJ/kg, J/kg)
n	rotational speed (rpm)
v	specific volume (m^3/kg)
u	peripheral speed (m/s)
x	velocity ratio
U	uncertainty
$\dot{m}$	mass flow rate (kg/s)
$\dot{P}$	power (kW)
$\dot{Q}$	Evaporator heat transfer rate (kW)
LFL	low flame limit (%)
ODP	Ozone depression potential
GWP	Global warming potential (100 yr)
ORC	organic Rankine cycle
1, 2, 3, 4, 5, 6, 7	state points of ORC
Greek letters	
η	efficiency
Subscripts	
c	critical
b	boiling
p	isobaric
trans	transmission
ge	generation
isen	isentropic
tur	turbine
ther	thermal
evap	evaporating
cond	condensing
Superscripts	
$'$	inlet
$''$	outlet

References

1. Tchanche, B.F.; Papadakis, G.; Lambrinos, G.; Frangoudakis, A. Fluid selection for a low-temperature solar organic Rankine cycle. *Appl. Therm. Eng.* **2009**, *29*, 2468–2476. [CrossRef]
2. Rayegan, R.; Tao, Y.X. A procedure to select working fluids for Solar Organic Rankine Cycles (ORCs). *Renew. Energy* **2011**, *36*, 659–670. [CrossRef]
3. Hettiarachchi, H.M.; Golubovic, M.; Worek, W.M.; Ikegami, Y. Optimum design criteria for an Organic Rankine cycle using low-temperature geothermal heat sources. *Energy* **2007**, *32*, 1698–1706. [CrossRef]
4. Shu, G.; Zhao, M.; Tian, H.; Huo, Y.; Zhu, W. Experimental comparison of R123 and R245fa as working fluids for waste heat recovery from heavy-duty diesel engine. *Energy* **2016**, *115*, 756–769. [CrossRef]
5. Pang, K.; Chen, S.; Hung, T.; Feng, Y.; Yang, S.; Wong, K.; Lin, J. Experimental study on organic Rankine cycle utilizing R245fa, R123 and their mixtures to investigate the maximum power generation from low-grade heat. *Energy* **2017**, *133*, 636–651. [CrossRef]
6. Wang, E.H.; Zhang, H.G.; Fan, B.Y.; Ouyang, M.G.; Zhao, Y.; Mu, Q.H. Study of working fluid selection of organic Rankine cycle (ORC) for engine waste heat recovery. *Energy* **2011**, *36*, 3406–3418. [CrossRef]
7. Dai, Y.P.; Wang, J.F.; Gao, L. Parametric optimization and comparative study of organic Rankine cycle (ORC) for low grade waste heat recovery. *Energy Convers. Manag.* **2009**, *50*, 576–582. [CrossRef]

8. Lakew, A.A.; Bolland, O. Working fluids for low-temperature heat source. *Appl. Therm. Eng.* **2010**, *30*, 1262–1268. [CrossRef]
9. Guo, T.; Wang, H.X.; Zhang, S.J. Comparative analysis of CO_2-based transcritical Rankine cycle and HFC245fa-based subcritical organic Rankine cycle (ORC) using low-temperature geothermal source. *Sci. China Technol. Sci.* **2010**, *53*, 1869–1900. [CrossRef]
10. Chen, H.; Goswami, D.Y.; Rahman, M.M.; Stefanakos, E.K. Energetic and exergetic analysis of CO_2- and R32-based transcritical Rankine cycles for low-grade heat conversion. *Appl. Energy* **2011**, *88*, 2802–2808. [CrossRef]
11. Zhang, X.; Yamaguchi, H.; Uneno, D. Experimental study on the performance of solar Rankine system using supercritical CO_2. *Renew. Energy* **2007**, *32*, 2617–2628. [CrossRef]
12. Yamaguchi, H.; Zhang, X.R.; Fujima, K.; Enomoto, M.; Sawada, N. Solar energy powered Rankine cycle using supercritical CO_2. *Appl. Therm. Eng.* **2006**, *26*, 2345–2354. [CrossRef]
13. Kim, Y.M.; Kim, C.G.; Favrat, D. Transcritical or supercritical CO_2 cycles using both low- and high-temperature heat sources. *Energy* **2012**, *43*, 402–415. [CrossRef]
14. Garg, P.; Kumar, P.; Srinivasan, K.; Dutta, P. Evaluation of carbon dioxide blends with isopentane and propane as working fluids for organic Rankine cycles. *Appl. Therm. Eng.* **2013**, *52*, 439–448. [CrossRef]
15. Pan, L.; Wang, H.; Shi, W. Performance analysis of a zeotropic mixture (R290/CO_2) for trans-critical power cycle. *Chin. J. Chem. Eng.* **2015**, *23*, 572–577. [CrossRef]
16. Pan, L.; Shi, W. Investigation on the pinch point position in heat exchangers. *J. Therm. Sci.* **2016**, *25*, 258–265. [CrossRef]
17. Pan, L.; Wang, H. Improved analysis of Organic Rankine Cycle based on radial flow turbine. *Appl. Therm. Eng.* **2013**, *61*, 606–615. [CrossRef]
18. Quoilin, S.; Aumann, R.; Grill, A. Dynamic modeling and optimal control strategy of waste heat recovery organic Rankine cycles. *Appl. Energy* **2011**, *88*, 2183–2190. [CrossRef]
19. Bamgbopa, M.O.; Uzgoren, E. Numerical analysis of an organic Rankine cycle under steady and variable heat input. *Appl. Energy* **2013**, *107*, 219–228. [CrossRef]
20. Zhang, J.; Zhou, Y.; Li, Y.; Hou, G.; Fang, F. Generalized predictive control applied in waste heat recovery power plants. *Appl. Energy* **2013**, *102*, 320–326. [CrossRef]
21. Palagi, L.; Pesyridis, A.; Sciubba, E.; Tocci, L. Machine Learning for the prediction of the dynamic behavior of a small scale ORC system. *Energy* **2019**, *166*, 72–82. [CrossRef]
22. Wang, J.L.; Zhao, L.; Wang, X.D. An experimental study on the recuperative low temperature solar Rankine cycle using R245fa. *Appl. Energy* **2012**, *94*, 34–40. [CrossRef]
23. Wang, X.D.; Zhao, L.; Wang, J.L.; Zhang, W.Z.; Zhao, X.Z.; Wu, W. Performance evaluation of a low-temperature solar Rankine cycle system utilizing R245fa. *Sol. Energy* **2010**, *84*, 353–364. [CrossRef]
24. Pan, L.; Wei, X.; Li, B.; Li, T. Experimental investigation on the CO_2 transcritical power cycle. *Energy* **2016**, *95*, 247–254. [CrossRef]
25. Gu, W. Theoretical and Experimental Study of Organic Rankine Cycle for Low and Medium Grade Heat Source Utilization. Ph.D. Dissertation, Shanghai Jiao Tong University, Shanghai, China, 2009.
26. Guo, T. Optimization on Combined Heat and Power System Powered by Moderately Low-Temperature Geothermal Sources. Ph.D. Dissertation, Tianjin University, Tianjin, China, 2011.
27. Zhou, N.; Wang, X.; Chen, Z.; Wang, Z. Experimental study on Organic Rankine Cycle for waste heat recovery from low-temperature flue gas. *Energy* **2013**, *55*, 216–225. [CrossRef]
28. Quoilin, S.; Lemort, V.; Lebrun, J. Experimental study and modeling of an organic Rankine cycle using scroll expander. *Appl. Energy* **2010**, *87*, 1260–1268. [CrossRef]
29. Declaye, S.; Quoilin, S.; Guillaume, L.; Lemort, V. Experimental study on an open-drive scroll expander integrated into an ORC (Organic Rankine Cycle) system with R245fa as working fluid. *Energy* **2013**, *55*, 173–183. [CrossRef]
30. Sauret, E.; Rowlands, A.S. Candidate radial-inflow turbines and high-density working fluids for geothermal power systems. *Energy* **2011**, *36*, 4460–4467. [CrossRef]
31. Fiaschi, D.; Manfrida, G.; Maraschiello, F. Thermo-fluid dynamics preliminary design of turbo-expanders for ORC cycles. *Appl. Energy* **2012**, *97*, 601–608. [CrossRef]
32. Pei, G.; Li, J.; Li, Y.; Wang, D.; Ji, J. Construction and dynamic test of a small-scale organic Rankine cycle. *Energy* **2011**, *36*, 3215–3223. [CrossRef]

33. Kang, S.H. Design and experimental study of ORC (organic Rankine cycle) and radial turbine using R245fa working fluid. *Energy* **2012**, *41*, 514–524. [CrossRef]
34. Manfrida, G.; Pacini, L.; Talluri, L. An upgraded Tesla turbine concept for ORC applications. *Energy* **2018**, *158*, 33–40. [CrossRef]
35. Talluri, L.; Fiaschi, D.; Neri, G.; Ciappi, L. Design and optimization of a Tesla turbine for ORC applications. *Appl. Energy* **2018**, *226*, 300–319. [CrossRef]
36. Calm, J.M.; Hourahan, G.C. Refrigerant data summary update. *HPAC Eng.* **2007**, *79*, 50–64.
37. Lemmon, E.W.; Huber, M.L.; McLinden, M.O. *NIST Standard Reference Database 23, Reference Fluid Thermodynamic and Transport Properties (REFPROP)*; version 9.0.; National Institute of Standards and Technology: Gaithersburg, MD, USA, 2010.
38. Pan, L.; Wang, H. Regulation law of turbine and generator in organic Rankine cycle power generation experimental system. *Trans. Tianjin Univ.* **2014**, *20*, 237–242. [CrossRef]
39. She, W.D.; Jiang, Z.M.; Tong, J.G. *Engineering Thermodynamics*; Higher Education Press: Beijing, China, 1982.